FACULTY OF SCIENCE AND TECHNOLOGY

# BACHELOR'S THESIS

| | |
|---|---|
| Study program / specialization:<br>Chemical and Environmental Engineering - Bachelor | Spring 2023<br>Open / Confidential |
| Author:<br>Haris Karunagaran | |
| Supervisor at UiS:<br>Sachin Maruti Chavan<br>Co-supervisor:<br>Widuramina Sameendranath Amarasinghe | |
| Thesis title:<br>Recovery and separation of critical metals for clean energy application | |
| Credits (ECTS):<br>20 | |
| Keywords:<br>Critical metals, Adsorption, MOF, UiO-66 and UiO-66-EDTA | Pages: 41<br>+ appendix: 8<br>Stavanger, *15th May 2023* |

# Recovery and separation of critical metals for clean energy application

By Haris Karunagaran

Bachelor of science
University of Stavanger

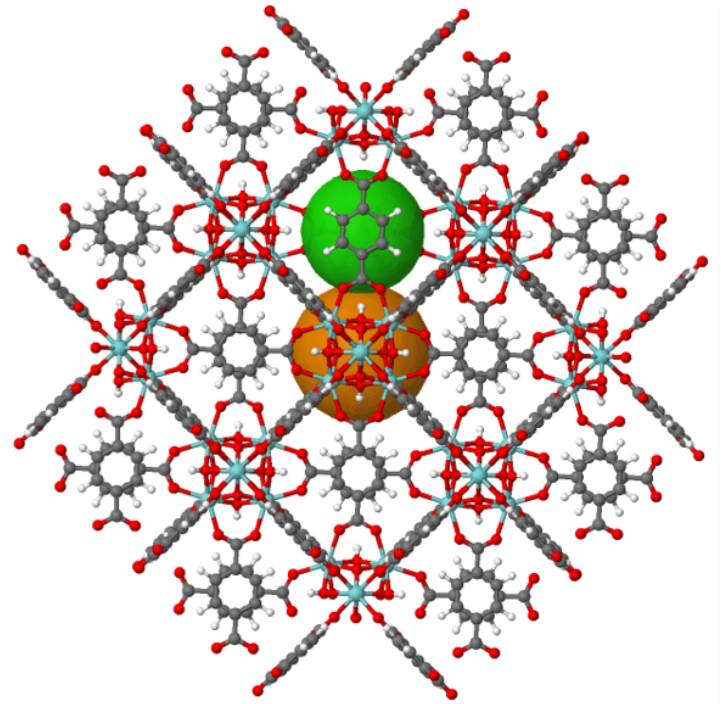

# ABSTRACT

The increase in demand and supply of critical metals for clean energy applications has led to a significant interest in the development of sustainable and efficient technologies for the recovery and separation of critical metals. Thus, the motive of this study was to perform synthesis, characterization, and adsorption performance for a promising adsorbent material, MOFs (Metal-Organic Framework), with the objective to recover and separate the critical metals such as lithium, magnesium, cobalt, and nickel, using batch adsorption.

UiO-66 and UiO-66-EDTA are the adsorbent materials that was chosen for this study owing their promising surface area, crystal structure, thermal stabilities etc. To confirm their characteristics several methods, such as XRD, TGA, $N_2$ sorption, SEM-EDS and NMR were conducted. The batch adsorption experiments were conducted to determine the metal uptake and selectivity of the critical metals focused on this study. UiO-66-EDTA displayed the highest uptake for the divalent cations,

# ACKNOWLEDGMENTS

This is the end of my bachelor's in chemical and environmental engineering on that occasion I would like to thank the University of Stavanger, the department of chemistry, bioscience, and environmental engineering. A huge thanks to my thesis supervisor Associate Professor Sachin M. Chavan, and PhD. students Simmy Rathod and Senith Fernando.

I am truly grateful for your time and effort you have invested in helping me achieve my potential. Your insightful feedback and constructive criticism have significantly helped the direction of my research and strengthened the overall quality of my bachelor thesis.

Your individual attention during our meetings and discussions has developed critical research skills, and analytical thinking, and brought a deeper understanding of the subject. Your guidance has not only contributed to the success of my thesis, but as a whole enriched my academic journey.

Finally, I would also like to thank my family and friends for motivating and supporting me during this time.

With warm regards, have a nice read.

Haris Karunagaran

# ABBREVIATIONS

| | |
|---|---|
| BET | Brauner-Emmett-Teller |
| EDS | Energy Dispersive Spectroscopy |
| EDTA | Ethylenediaminetetraacetic acid |
| LIB | Lithium-Ion Battery |
| MOF | Metal Organic Frameworks |
| NMR | Nuclear Magnetic Resonance |
| PXRD | Powder X-Ray Diffraction |
| PPM | Parts per Million |
| RPM | Rotation per minute |
| SEM | Scanning Electron Microscopy |
| TGA | Thermogravimetric Analysis |
| UiO | Universitetet i Oslo |

# TABLE OF CONTENTS

# 1 INTRODUCTION

The globe is shifting toward sustainable, clean, and resource-conserving energy. The transition to clean energy is essential for mitigating climate change and reducing reliance on fossil fuels. For this to be viable, it is necessary to have access to critical metals that are essential for batteries, wind and solar energy, fuel cells, and most crucial industrial chemical processes. These metals are frequently irreplaceable due to their scarcity and effectivity which is a reality requiring long-term attention.

To overcome these limitations, several innovative and eco-efficient processes have been researched and developed to recover and separate critical metals from various sources, including membrane filtration, chemical coagulation, hydrometallurgy, bioleaching, solvent, ion exchange, electrochemical deposition, and adsorption are gaining significant attention to recover critical metals from mining and electronic waste. These processes aim to minimize environmental impact, reduce energy consumption, and ensure a sustainable supply chain for clean energy technologies.

Among these technologies the most popular technology is adsorption due to its many benefits such as simplicity, ease of preparation, cost effectiveness, and exceptional removal performance. As a result, numerous adsorbents have been developed to purify critical metals. (ACS Sustainable Chemistry and Engineering, 2017).

Metal-organic frameworks (MOFs) are some of the adsorbents which have been under extensive academic study over the past 20 years and are emerging on the industrial scale. Despite these progresses, one general challenge, existing MOFs still face, is the specificity in metal removal. It means that these MOFs are effective in the removal of one or many target metal ions, while they show poor performance in the treatment of some other metal ions.

# 2 LITERATURE REVIEW AND THEORY

## 2.1 CRITICAL METALS

A metal is considered critical if issues with its supply could have negative effects on the industry or the economy. Most international studies use two factors to determine the criticality of metals:

Supply risks are calculated based on factors that measure the risk of disruptions in the supply of a given material, e.g., supply concentration of production in countries with poor governance performance, trade restrictions and agreements, import reliance, and existence and limited material substitutability.

Economic importance are calculated based on the importance of a given material for end-use applications and on the performance of its substitutes in those applications, which measures how vulnerable the economy is to a potential shortage or supply interruption (*Critical Raw Materials*, u.å.).

Of all the critical raw metals, there are 30 metals with are labeled as critical, based on the two factors explained above. Some of the critical raw metals, according to the EU, include lithium (Li), cobalt (Co), magnesium (Mg), heavy rare earth elements, light rare earth elements, and platinum group elements.

## 2.2 DEMAND AND SUPPLY OF CRITICAL METALS

The demand for critical metals is increasing daily, pushing several metals to the brink of supply danger. They serve a crucial role in the creation of high-tech materials used in fields including sustainable materials engineering, renewable energy, and cleaner production, with their unique physical and chemical properties.

### *2.2.1 Demand*

Critical metal demand is predominantly driven by the expansion of secondary resources, in the battery industry. Therefore, the recovery of lithium from primary and secondary resources has attracted much attention to either meet lithium requirements or minimize waste disposal problems (Swain, 2017).

Many of these materials are currently only extracted in a few countries, which increases the risk of supply shortages and supply vulnerability. The likelihood of supply disruption is

further increased by the fact that processing, smelting, and refining of many metals are also concentrated in a small number of countries, according to a document prepared for the European Commission.

### *2.2.2 Primary sources*

The purest critical metals are produced from mining, steel processing, or metallurgy processes, They are generally found in a variety of natural reservoirs, primary sources, such as ores, minerals, clays, salt lakes, and underground brine reservoirs, which are the primary sources for all commercial production (Costa et al., 2021). The depletion of those primary resources for critical metals is one of the most important environmental and societal challenges nowadays.

The possible reported process for extraction of metals from the waste is pyrometallurgy, hydrometallurgy, and bio-metallurgy. In hydrometallurgy, the metal leaches out from the primary source using an aqueous chemical, and the resulting solution is called leachate. The critical part is the separation of metals from multi-metallic containing leachate using well-crafted adsorbents.

### *2.2.3 Secondary sources*

Electronic waste, which is typically generated from manufacture of electrical and electronic equipment, energy production and waste management, are important secondary resources. The promotion of critical metal recovery or electronic waste treatment to be green and sustainable involves technological advances and breakthroughs in process design in addition to the current practices of recycling electronic waste.

## 2.3 RECOVERY OF SECONDARY CRITICAL METALS

As mentioned above, there are increased research to recover critical metals, especially from secondary resources by eco-efficient processes (Gavrilescu, 2022). The increasing demand of Lithium-Ion-Batteries, mainly driven by implementation of electric vehicles, brings several environmental issues related to the mining, extraction, and purification of scarce materials such as lithium, cobalt and nickel. The presence of limited resources can lead to break in the chain of supply of these metals on demand. Therefore, it is necessary to recycle lithium, cobalt, and nickel from secondary resources to continue the chain of demand and supply (Alvial-Hein et al., 2021).

### *2.3.1 Lithium (Li)*

Lithium as the lightest metal element in the periodic table, possesses unique properties including excellent chemical activity, high specific heat, and a low expansion coefficient (Tapia-Ruiz et al., 2013). Lithium (Li(I)) exists in leaching solution as a cationic species with other metal ions such as Na(I), K(I), Ca(II), Mg(II), etc. These metals have nearly identical ionic radiuses and thus the separation of Li(I) from the leaching solutions becomes more difficult.

Therefore, finding commercial extractants with a low cost and high extraction efficiency is needed for the recovery of Li(I) from secondary resources. Some review papers have been published on recovery of lithium from secondary sources. However, little data has been reported in these review papers on the solvent extraction of Li(I) from these leaching extractions (Meshram et al., 2014).

At present no lithium extraction is industrially practiced from LIBs. Therefore, a sufficient scope exists not only to reduce the process steps followed currently but also to improve the efficiency of metal extraction and separation, including lithium recovery (Meshram et al., 2014).

### *2.3.2 Cobalt (Co) and Nickel (Ni)*

Cobalt and nickel are essential “transition” metals, which are used in various applications, such as rechargeable batteries e.g., LIB and NiMH. Both Co (II) and Ni(II) exist as divalent ions and have similar chemical and physical properties, which makes it difficult to separate them individually. Currently, recovery of these metals is of particular interest due to their specific properties such as high melting and boiling points, hardness, electrical and

thermal conductivity, variable oxidation states, magnetism, and tendency to form alloys with other elements.

### *2.3.3 Magnesium (Mg)*

Magnesium is another critical metal of which has exceptionally large economic importance. The importance comes from the increase in risk of supply shortages and vulnerability along the value chain. Several countries including China, which is the major EU supplier of CRMs, are the reason behind these risks.

## 2.4 RECYCLING OF CRITICAL METALS

For metals in general, recycling practices are well established, but this is not yet the case for many energy-transition metals such as lithium and other critical metals. Recycling of these metals is important in view of the efficient use of natural resources and to ensure a supply of these critical raw materials. The balance problem (Falconnet, 1985), includes the demand and supply of the individual rare-earth metals to be equal at any time, to relieve the pressure on primary resources. Otherwise, there will be shortages or excesses of some elements.

## 2.5 SEPARATION PROCESSES

Among available approaches for separation processes, such as distillation, crystallization, extraction, absorption, adsorption, and membrane separations, adsorptive separation is used for metal contaminants removal due to multiple merits such as simplicity, high availability, and exceptional removal performances. Adsorptions refer to the process by which a mixture is separated based on differences in adsorption/desorption behavior of distinct components in the mixture.

### *2.5.1 Adsorption*

Adsorptive processes are created from the differences in adsorption behaviors of mixture components which are directly related to adsorbent properties in terms of adsorption equilibria and kinetics. The two main characteristics of an adsorbent relevant to adsorptive separation are its adsorption capacity and selectivity. The nature of the pores in the adsorbent as well as the working circumstances, such as temperature and pressure in gas separations and solvent system in liquid separations, influence the process. (Li et al., 2012)

### *2.5.2 Adsorption with MOFs*

The adsorption technology mainly depends on the properties of adsorbents (functional groups, specific surface area, etc.), in which MOFs are feasible candidates as medium materials in adsorption. Compared to other adsorbents, MOFs have a higher degree of designability and adjustability in their structures and functions, when compared to other porous solid materials.

## 2.6 MOF STRUCTURE

Metal-Organic Frameworks (MOFs) are crystalline porous materials composed of coordinated bonds (reticular synthesis) between metal clusters and organic linkers, the interaction of which controls the pore sizes and shape of the MOF. The flexibility with which metal clusters and organic linkers can be varied has led to thousands of compounds being prepared and studied. Unlike other extended solids, MOFs maintain their underlying structure and crystalline order upon expansion of organic linkers and inorganic secondary building units (SBUs), as well as after chemical functionalization, which significantly widens the scope of this chemistry (Furukawa et al., 2013).

The synthesis of MOFs is usually carried out at mild conditions, which means that the synthetic conditions are easily controlled. Organic ligands can be efficiently designed and modified using the power of organic synthesis. Due to the fixed coordination geometries of both organic ligands and metal ions, a particular combination of rigid organic and inorganic building units always produces a specific framework. Within a narrow definition of MOFs, using the reticular synthesis approach can tune the structures and properties of MOFs without changing the connectivity or topology through the pre-synthesis design of ligands, SBUs, and synthetic conditions. MOFs can be modified at the metal nodes or the organic linker after synthesis.

### *2.6.1 Zirconium based MOFs*

The viability of synthesizing and functionalizing a MOF, for use in industrial processes must be considered. The synthesis must be reasonably priced, reliable, scalable, and ideally sustainable. Options that meet several of these characteristics are offered by some MOFs.

Zirconium-based MOFs (Zr-MOFs) in particular, stand out due to their enormous specific surface area, outstanding thermal and chemical stability, and notable catalytic properties in various reactions. appear to be viable options (Aunan et al., 2021). Since Zirconium and the rest of group four elements in the periodic table have strong interaction with oxygen and hence, makes them clear choices for stable inorganic foundations when used with oxygen containing linkers.

### *2.6.2 UiO-66*

The whole interest in Zr-MOFs peaked, with the discovery of UiO-66 ($Zr_6O_4(OH_4)(BDC)_6$) (Cavka et al., 2008). Since then, because to their ground-breaking stability, they have maintained an ideal standard for groundbreaking MOFs. This stability is derived from each zirconium unit which are connected by 12 ditopic linkers (terephthalic acid, $H_2BDC$), that is provided by the strong Zr-O bond.

MOFs of UiO-66 ($Zr_6O_4(OH)_4(CO_2C_6H_4CO_2)_6$) has gained much attention owing to its great chemical stability, high working capacity, easy separation, and facile modifiability, which allows for its further applications in different fields including gas adsorption, catalysis, energy storage, biomedical and effluents treatment. The theoretical pore volume of UiO-66 is 0.77 $cm^3/g$, and the surface area is 1160 $m^2/g$ (Ghosh et al., 2014; H. Wu et al., 2013).

### *2.6.3 Modification of UiO-66*

The MOF in general was discovered to be extremely stable but highly inert, so its performance was not exceptional. Compared to other adsorbent, MOFs organic linkers can be quickly functionalized using a variety of techniques, such as direct solvothermal synthesis and post-synthetic methods. These processes have a common designation called modification. UiO-66-COOH, UiO-66-$NH_2$, UiO-66-$NO_2$ and UiO-66-EDTA are some common modifications of UiO-66.

UiO-66-EDTA is a modified UiO-66 in which ethylenediaminetetraacetic acid (EDTA) ligands have taken the place of some of the terephthalate linkers, that possess high chemical stability, facile synthesis method, efficient removal performance and superior reusability (J. Wu et al., 2019),

# 3 THESIS OBJECTIVE

Recovery and recycling of critical metals from spent battery waste electrode materials is a timely topic of interest. Much research has been conducted to leach and recover most of the elements. The recovery efficiencies of primary resources have reached an optimized condition, but the separation efficiencies of the critical metals are still at a lower level.

The studies and conducted processes are focused on those metals. Therefore, the research area to investigate an efficient, environmentally sustainable metal recovery and separation process to provide raw materials to make a high-quality reusable metal is still an open and challenging study to work on.

The primary objective of this project is to synthesis UiO-66 and UiO-66-EDTA for the adsorption-enhanced recovery of critical metals, such as monovalent metal lithium ($Li^{+}$), and divalent metals magnesium ($Mg^{2+}$), cobalt ($Co^{2+}$), and nickel ($Ni^{2+}$).

Then characterize them with the intention of minimize the utilization of energy and chemicals, which can be applied to the industrial processes by increasing the amount of recovery and recycling for those metals. Additionally, increase the proportion of clean energy technology in the energy industry and secure the supply underpinned by the circular economy.

# 4 MATERIALS AND METHODS

## 4.1 MATERIALS

| Chemicals | Name | Producer | CAS NO. |
|---|---|---|---|
| $ZrCl_4$ | Zirconium (IV) tetrachloride | Sigma-Aldrich | 10026-11-6 |
| DMF | N, N-dimethylformamide | Supelco | 68-12-2 |
| $H_2BDC$ | Terephthalic acid | Sigma-Aldrich | 100-21-0 |
| $H_2O$ | Distilled water | University of Stavanger, faculty for chemistry | |
| | Millipore water | | |
| EDTA | Ethylenediaminetetraacetic acid | Merck | 60-00-4 |
| LiCl | Lithium chloride | VWR | 7447-41-8 |
| $MgCl_2 \cdot 6H_2O$ | Magnesium chloride hexahydrate | VWR | 7791-18-6 |
| $NiCl_2 \cdot 6H_2O$ | Nickel (II) chloride hexahydrate | Sigma-Aldrich | 7791-20-0 |
| $CoCl_2 \cdot 6H_2O$ | Cobalt (II) chloride hexahydrate | Sigma-Aldrich | 7791-13-1 |
| NaOH | Sodium hydroxide (98.7%) | VWR | 1310-73-2 |
| HCl | Hydrochloride acid (35.7%) | VWR | 7647-01-0 |

Table 4-1. Chemicals used for the synthesis and modification of UiO-66, preparation of simulated and adsorption solutions

## 4.2 SYNTHESIS AND PREPARATION

### *4.2.1 Synthesis of UiO-66*

The UiO-66 synthesis method was obtained and optimized by the ideal UiO-66 procedure from (Shearer et al., 2016)). All chemicals were purchased from commercial vendors and used without being purified further. Firstly, two 500 mL volumetric flasks were rinsed with DMF, before the reaction mixtures were prepared by dissolving 2.5 g (1 eqv.) of $ZrCl_4$ in 291 mL (350 eqv.) of DMF, in each flask. 251 µL (1.3 eqv.) of deionized water was added, before adding 1.7828 g (1 eqv.) of $H_2BDC$ and dissolved on a hot plate at 80 °C using a magnet stirrer at 220 RPM. Then the flasks were sealed and placed in a 100 °C oven for 72 hours to perform the synthesis under static conditions.

| | Molar weight (g/mol) | Density (g/ml) | Actual amount | | Molar ratio |
|---|---|---|---|---|---|
| | | | A | B | |
| $ZrCl_4$ | 233.04 | - | 2.5080 g | 2.5067 g | 1 |
| $H_2BDC$ | 166.13 | - | 1.7828 g | 1.7828 g | 1 |
| DMF | 73.09 | 0.944 | 290.71 mL | 290.71 mL | 350 |
| $H_2O$ | 18.02 | 1.000 | 0.251 mL | 0.2513 mL | 1.3 |

Table 4-2 Reagents quantities used for the synthesis of UiO-66.

The resulting products precipitated as microcrystalline powders, to obtain that they were centrifuged and washed twice in DMF (30 mL) while being stirred for 1 hour at 150 RPM each time. Then they were washed once more with 30 mL DMF and stirred overnight at the same RPM. The materials were washed three times in 150 ml distilled water at 80 °C for two hours each time to obtain water exchanged samples. Finally, all the samples were dried at 60 °C in air for 24 h.

### *4.2.2 Synthesis of UiO-66-EDTA*

In a screw capped glass bottle, respective quantities of EDTA and NaOH (amount shown in Table) was added to distilled water. The mixture was stirred until clear solution. An appropriate quantity of activated UiO-66 was added to the mixture above. The mixture was then heated at 60°C for 24 hrs under stirring. The product was obtained through filtration. It was then washed several times with water to remove unreacted EDTA. To exchange water in the MOF, it was then washed several times with acetone. The product was then dried in an oven overnight at 60°C.

| | Molar weight (g/mol) | mmol | Density (g/ml) | Actual amount taken | Molar equivalent |
|---|---|---|---|---|---|
| UiO-66 | 1664.08 | 0.9014 | - | 1.50 g | 1 |
| 2Na-EDTA | 292.24 | 82.9287 | - | 24.235 g | 92 |
| NaOH | 39.997 | 165.8572 | 2.130 | 6.634 g | 184 |
| $H_2O$ | 18.02 | 36.1605 | 1.000 | 652 mL | 40.116 |

Table 4-3 Reagents quantities used for the synthesis of UiO-66-EDTA

## 4.3 CHARACTERIZATION METHODS

The synthesized UiO-66, UiO-66-EDTA and UiO-66-EDTMP were characterized using the methods such as PXRD, TGA, SEM-EDS, $N_2$ sorption and NMR for studying accordingly the crystal structures, thermal stabilities, surface functional groups, surface areas, and the loading of functional groups.

### *4.3.1 X-ray diffraction (XRD)*

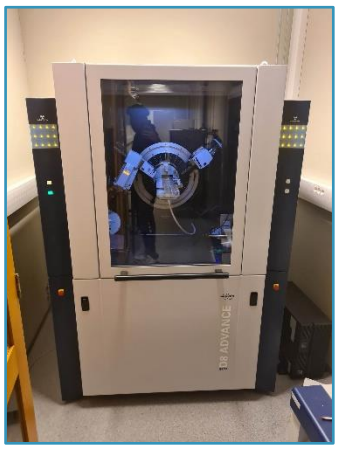

Figure 4-1. XRD instrument to characterize the crystal structure

XRD was applied to characterize the crystallinity of the material and to confirm the crystalline nature of synthesized MOF, by comparing it with simulated version of the MOF. The cathode ray tube generates X-rays with are transformed into monochromatic radiation and directed at the sample. The sample is scanned at various 2θ degree angles, and the diffracted X-rays are identified and counted to generate intensity values at each 2θ degree angle (Li et al., 2012).

The procedure of conducting XRD analysis begins with dispersing a quantity of more than 500 mg of powdered sample on a flat, glass plate PXRD sample holder with a diameter of 2.5 cm. The powdered sample was distributed evenly on the sample holder using a blade and smoothened. A thin glass plate was then used to spread to flatten and hold the sample in position for measurement. For samples in smaller quantities, ethyl alcohol was used to make a slurry, which was then applied drop by drop to the sample container and dried until a thin powder coating developed.

The sample holders were put on the D8 Advance-Bruker XRD sample stage and scanned from 2° to 70° 2θ at a short-run scan speed of 5.77° $min^{-1}$ and a long-run scan speed of 1.19° $min^{-1}$. A Cu-Kα radiation source with a wavelength (λ) of 1.5418 Å was used for the

study. The X-ray tube was powered by a voltage of 40 kV and a current of 25 mA. Data was received in XY-file format, and QtiPlot was used to create graphs.

### *4.3.2 Thermogravimetric analysis (TGA)*


Figure 4-2. TGA instrument used to assess the thermal stability

TGA analysis was used to assess the thermal behavior of physical properties such as sample mass by varying the sample temperature against time on a Mettler Toledo TGA/DSC 3+ STARe system. The sample moisture content, component decompositions, and removals can all be estimated using the sample mass variation with temperature.

The following is the procedure for performing TGA analysis. Firstly, an empty 70 µL alumina oxide ($Al_2O_3$) crucible was placed on the sample position and tared. In the alumina crucible, approximately 10 mg of the sample was placed. By tapping the crucible on a table, the sample surface in the alumina crucible was leveled and packed. The experiment was carried out with a heating rate of 5 (°C/min) from 25 °C to 900 °C in a synthetic airflow of 25 (mL/min). The sample weight was determined using the first weight measurement. The data was obtained in the form of an XY-file, and plots were created with QtiPlot.

### *4.3.3 Scanning electron microscope-energy dispersive spectrometer (SEM-EDS)*

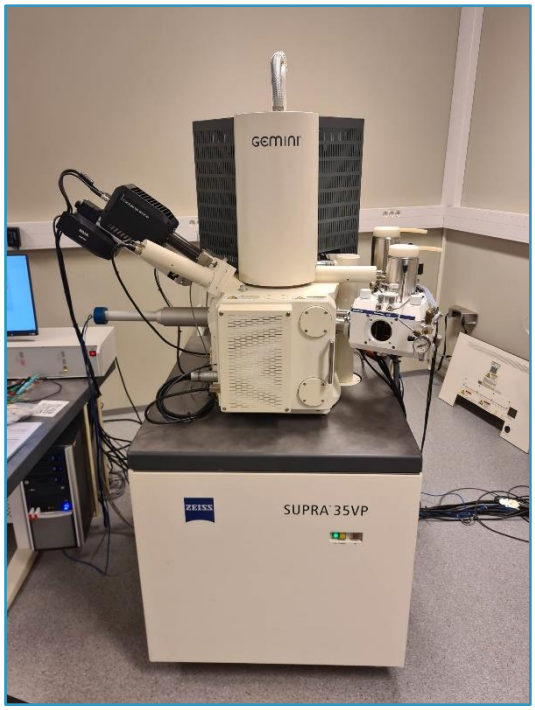


Figure 4-3. SEM-EDS instrument used to analyze the particle shape and elemental composition

Zeiss SUPRA 35VP (SEM) and EDAX energy dispersive spectroscopy (EDS), were used to analyze and examine, the particle shape and elemental composition of the samples. SEM-EDS analysis is a non-destructive analytical technique in which the sample is exposed to electron radiation to cause the emission of individual X-rays from the elements. The emitted energies are shown as a spectrum, with the peaks designating the strength of the various elements.

The procedure for carrying out the analysis were as follows. First, a finely powdered sample was glued, on a carbon tape that was attached to the sample holder, and then the unattached sample on the tape was gently cleared out with a hairdryer. The samples were put inside the apparatus, viewed with a SEM at a magnification of 500–5000, and different spots and regions were investigated with an EDS to determine their elemental composition. The results from the SEM and EDS were acquired in in the image file and doc file format, respectively.

### *4.3.4 Nitrogen sorption analysis*


Figure 4-4. (A) $N_2$ sorption instrument used to analyze the surface area (B) Degassing unit with samples placed on heating positions

Nitrogen sorption was performed to analyze the surface area by Micromeritics TriStar II Plus. To conduct the analysis, nitrogen absorption is measured at 77 K with increasing relative pressure up to 1 bar. BET theory was used to compute the surface area. The sample that will be studied is cooled using liquid nitrogen, due to the weak interaction between gases and solids.

The procedure for the analysis was as follows. First the weight of the empty tube was measured, then for each sample, approximately 150 mg of sample was weighed into the tube. Prior to the BET measurement, the sample was degassed via simultaneous vacuum and heat treatment; first for 1 hour at 60 °C, then for 2 hours at 160 °C. The rubber cap was again used to cap the degassed sample, and the mass measured. The tubes were put into the BET instrument, and nitrogen sorption were conducted. The data were downloaded in .xls-files format and plotted using the Microsoft Excel program.

### *4.3.5 NMR*


Figure 4-5. NMR instrument used to quantify exchange and loading of ligands and functional groups

NMR was used to quantify the exchange and loading of the ligands and functional groups into UiO-66 and UiO-66-EDTA. The analysis was conducted by Bruker Ascend™ 400Hz NMR Spectrometer. 20 mg of MOF sample was weighed into a centrifuge tube and 1 mL of freshly prepared 1 M NaOH in $D_2O$ was added. The centrifuge tube was kept for 24 h for digestion, this procedure ensures that the organic compounds leach out of the MOF whereas the inorganic part settles at the bottom. Then the mixture was centrifugated to separate the suspension and transferred into the NMR tube for the analysis. The data were processed using TopSpin software, the peaks were integrated, and the protons were normalized in accord to the protons of trimesic acid.

## 4.4 BATCH ADSORPTION

This section presents the preparations of solution that are made for develop simulated calibration curve and the preparation of batch adsorption samples.

### *4.4.1 Preparation of solution for simulated calibration curve*

Initially, 250 ml of 2000 mg/$L^{-1}$ (PPM) of LiCl solution was prepared using 0.6108 g of LiCl in 250 ml millipore (Milli-Q) lab water. This solution was diluted in a series of concentrations; 50, 100, 250, 500, 750 and 1000 mg/$L^{-1}$ with millipore water. The diluted solutions were then inserted in IC and measured for making a simulated calibration curve. The solution for simulated calibration curve for nickel and cobalt was prepared and plotted by former master's student (Fernando, 2022), which is shown in Appendix V.

### *4.4.2 Batch adsorption samples for LiCl*

The procedure for the adsorption samples was as follows. First, a solution of 1000 mg/L LiCl was prepared in a 500 ml flask. 20 ml of the LiCl solution was then transferred to small vials for further adjustments. The pH was measure after adjusting using 1.0 M HCl (for pH 5), 0.1 M NaOH (for pH 8 to 10) and 1.0 M NaOH (for pH 11 and 12). 0.1 g MOF was then added to the vials the pH was recorded with a VWR phenomenal PH 1100 L after. The measured pH values before and after adding MOF for each sample is tabled in Appendix IV. The added MOFs were UiO-66 (mixed batch of 50% UiO-66-(A) and 50% UiO-66-(B)), and UiO-66-EDTA. In Table 2, the recorded pH before and after adding MOF are shown. All the vials were kept in a water bath at 25 °C for 24 hours under continuous stirring. After 24 hours, the adsorbed solutions were centrifuged and filtered using syringe and filter. The solutions were diluted 500 times and analyzed using ion chromatography.

### *4.4.3 Ion Chromatography (IC)*

Ion Chromatography (IC) Is a technique frequently used determine the ionic substances present in a sample. The IC-analysis were done for both the prepared simulated solution of $Li^{2+}$ and the batch adsorption samples. Before performing an IC analysis, all the solutions were diluted with GILSON GX-274 Liquid Handler, which ensures that the samples are in the appropriate concentration range for the IC instrument. The diluted samples were transferred to small vials with a syringe before inserting the samples in the instrument. To ensure the sample solution does not stick to the syringe, 2 ml of water was used to wet the syringe. Further on, 1 ml diluted solution was extracted to rinse the syringe. The remaining volume of diluted solution was then extracted and filtered until only around 1.2 ml solution

was left in the syringe. The remaining volume was then put into the small test tube and positioned in the IC instrument for analysis. The instrument for IC-analysis was performed using a Dionex ICS-5000.

### *4.4.4 Batch adsorption samples for $Co^{2+}$ and $Ni^{2+}$*

2000 mg/L of $Ni^{2+}$ and 600 mg/L of $Co^{2+}$, which corresponds to 1:5 diluted aqua regia digestion solution metal concentrations were prepared using 2.0876 g and 0.6057 g of $NiCl_2 \cdot 6H_2O$ and $CoCl_2 \cdot 6H_2O$ respectively in 250 mL of distilled water. Then the solutions of $Ni^{2+}$ and $Co^{2+}$ were 50 mg of UiO-66 and 50 mg of UiO-66-EDTA was measured and added to the vials. All the vials were kept in a water bath at 25 °C for 24 hours under continuous stirring. After 24 hours, the adsorbed solutions were centrifuged and filtered using syringe and filter.

### *4.4.5 UV-visible spectroscopy*

For UV-analysis an exceptionally instrument, UV-1600PC spectrophotometer, is utilized to determining the adsorption of $Co^{2+}$ and $Ni^{2+}$ with UiO-66 and UiO-66-EDTA. The spectrophotometer works by analyzing the light that is absorbed and transmitted from the metals. To conduct the adsorption analysis with the instrument a small amount of approximately 3.0 mL of the prepared solutions with $Co^{2+}$ and $Ni^{2+}$ was taken into a quartz cuvette. The cuvette was then put into the spectrophotometer and the spectrum was recorded from wavelength 190 nm to 900 nm. This procedure was performed for both the simulated solutions and the batch adsorption samples of $Co^{2+}$ and $Ni^{2+}$.

# 5 RESULTS AND DISCUSSION

## 5.1 MOF SYNTHESIS

The synthesis of both UiO-66 and the modified UiO-66-EDTA were successfully produced and resulted in a 90−95% yield of MOF material. The calculation for the missing linker defects and missing cluster defects are displayed in Appendix I.

## 5.2 CHARACTERIZATION OF UIO-66 AND UIO-66-EDTA

### *5.2.1 Crystal structure*

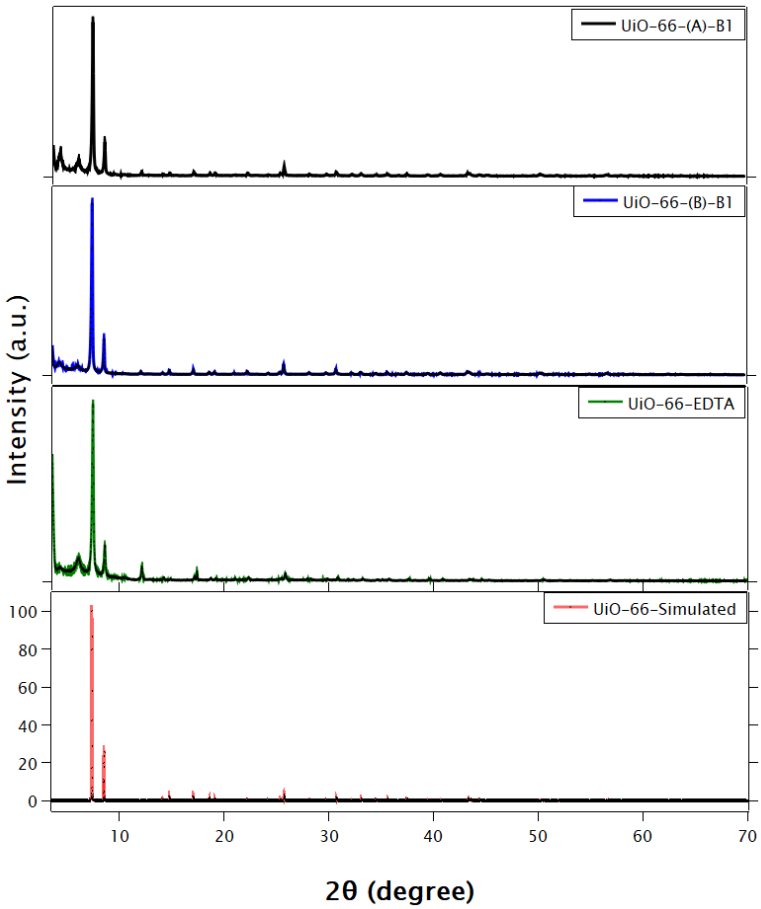


Figure 5-1 XRD pattern comparison of synthesized and simulated UiO-66, and UiO-66-EDTA

The XRD pattern for both UiO-66 batches and UiO-66-EDTA are shown above in Figure 5-1. The simulated diffraction data of UiO-66 was produced using a crystal information file (.cif) in VESTA software to compare and confirm the crystal structure of synthesized UiO-66 and UiO-66-EDTA. The plots show the intensity in y-axis and the diffraction angles in x-axis. The XRD patterns for synthesized UiO-66 and UiO-66-EDTA were normalized to the simulated curve by adjusting the intensity (y-axis).

The UiO-66-EDTA in a single modified batch was around 1.2 g. Since PXRD required a significant amount of the modified sample, therefore slurry sample of UiO-66-EDTA was prepared and analyzed. By comparing the diffraction peaks of the simulated UiO-66 with synthesized UiO-66 and the modified UiO-66-EDTA, there are two characteristics peaks located at 7.37° and 8.51° which corresponds respectively to the (111) and (200) planes of UiO-66. This confirmed the unchanged crystal structure after both synthesize and modification, based on the observation of corresponding peaks of MOFs which had peaks at almost the same 2θ angles.

The wavery small peaks of UiO-66 and UiO-66-EDTA compared to the simulated which had no peaks from 3.5° to 7° 2θ, identifies the missing cluster defects (Shearer et al., 2016) in the crystalline structure from substituted atoms, structural defects, or from thermal treatment.

### *5.2.2 Thermal stability*

The theoretical weight of UiO-66 and UiO-66-EDTA relative to the weight of the metal oxide product, 6 $ZrO_2$, were calculated and plotted onto the TGA plots. The theoretical weight percentages of the UiO-66 and the respective weight of 6 $ZrO_2$, were plotted as dotted lines in the TGA plots. Figure 5-2 below shows the TGA for both UiO-66 batches (A and B) and UiO-66-EDTA.

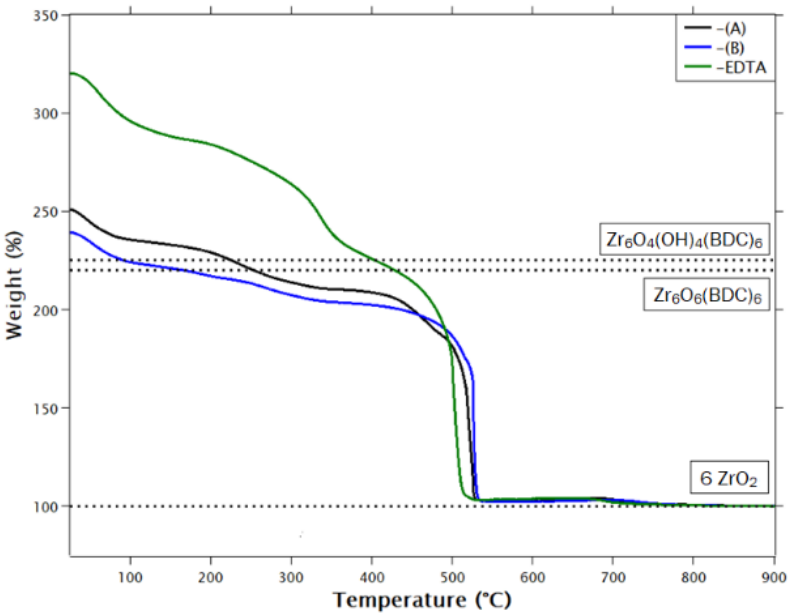


Figure 5-2. TGA comparison of UiO-66 and UiO-66-EDTA

The theoretical weight loss percentages can be calculated as follows, with respect to the weight of 6 $ZrO_2$:

Theoretical weight % of $Zr_6O_4(OH)_4(BDC)_6$:

$$\frac{Zr_6O_4(OH)_4(BDC)_6}{6\ ZrO_2} = \frac{1664.0607\frac{g}{mol}}{6 \times 123{,}22\frac{g}{mol}} \times 100\% = 225.08\%$$

Theoretical weight loss due to de-hydroxylation = 225.08% - 220.21% = 4.87%

Theoretical weight % of $Zr_6O_6(BDC)_6$:

$$\frac{Zr_6O_6(BDC)_6}{6\ ZrO_2} = \frac{(1664.0607 - 36{,}03056)\frac{g}{mol}}{6 \times 123.22\frac{g}{mol}} \times 100\ \% = 220.21\%$$

Theoretical weight loss % due to linker removal = 220.21% - 100% = 120.21%

The theoretical weight loss due to linker removal were slightly higher than that of respective experimental removal and the experimental de-hydroxylation was higher than the theoretical, which indicates the presence of missing linker defects in both UiO-66 batches and UiO-66-EDTA. The experimental values were calculated and the graph plotted, which is presented in Appendix I. According to the TGA, the activation temperature for UiO-66 was considered 160 °C, which removes the solvent and unreacted modulator content in the pores, which is 46.8 % with respect to the weight of 6 $ZrO_2$.

### *5.2.3 Morphology*

SEM and EDS was conducted to analyze both morphology and topography, and the composition of UiO-66-Batch:1 ((A) and (B)) and UiO-66-EDTA, respectively. Figure 5-3. displays the SEM images.

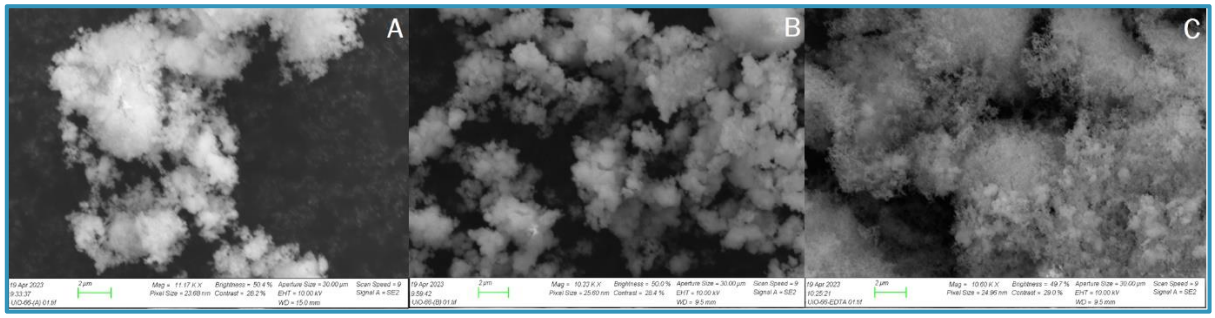


Figure 5-3. SEM micrographs of (A) UiO-66-(A) **left**, (B) UiO-66-(B) **middle** and (C) UiO-66-EDTA **right**

The SEM images provides information about the outer surface of the synthesized and modified UiO-66. EDS results presents the specter of elemental composition at the considered quite bulk portion of the sample for (A) UiO-66-(A), (B) UiO-66-B, and (C) for UiO-66-EDTA. The EDS spectrum of UiO-66, Figure 5-4. (A) and (B), shows that there is still a small amount of chlorine ions (0.29 wt% and 3.21 wt%) left in the sample, due to lack of washing, which indicates to chloride at the defect site, that is strongly bound to Zr therefore was not removed with washing at 80 °C. The spectrum of UiO-66-EDTA, Figure 5-4 (C), confirms the presences of nitrogen (39.90 atomic %), which validates the modified UiO-66 with EDTA. There is a slight peak for natrium which can explain to either unreacted EDTA (2Na-EDTA from modification) or deficiency from washing.

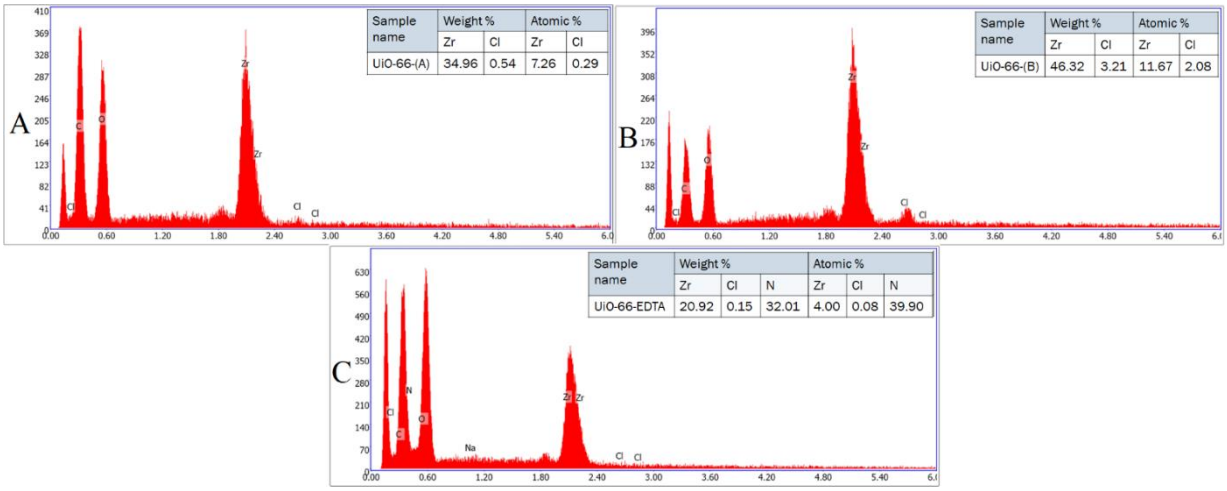


Figure 5-4. EDS analysis and summarized values of weight % and atom % for (A) UiO-66-(A) on **top-left**, (B) UiO-66-(B) on **top-right** and (C) UiO-66-EDTA on **bottom**

### *5.2.4 Surface area*

$N_2$ sorption isotherms for both UiO-66 ((A) and (B)) and modified UiO-66-EDTA, are shown below in Figure 5-5. The shape of these curves implies that UiO-66 and UiO-66-EDTA follows IUPAC type I isotherm, which is common for microporous adsorbents such as MOFs. The defining characteristic of IUPAC type I isotherm, is the adsorption capacity rises sharply at low pressures, followed by an equilibrium when the pores become saturated with $N_2$ molecules, which also corresponds to the UiO-66 and UiO-66-EDTA graphs.

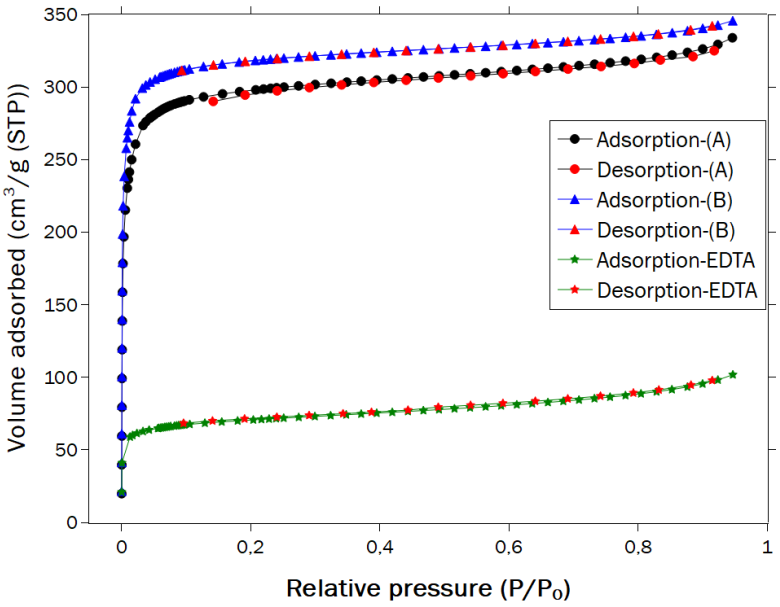


Figure 5-5. $N_2$ adsorption and desorption isotherms for UiO-66-(A) (**circle**), UiO-66-(B) (**triangle**) and modified UiO-66-EDTA (**star**)

A summarized results from the calculation of BET surface area, total pore volume, and monolayer pore volume for the three samples is provided below, in Table 5-1. The high correlation coefficient of 0.9995 for UiO-66-(A) and UiO-66-(B) indicates that the data from $N_2$ sorption fits the BET plots (in Appendix II). According to the correlation coefficient for UiO-66-EDTA at 1.0000, which implies that the data fits the BET plot model perfectly.

| Adsorbent | BET surface area ($m^2/g$) | Total pore volume ($cm^3/g$) at 0.94 $P/P_0$ | Monolayer pore volume ($V_m$ = $cm^3$ (STP)/g) | Correlation coefficient |
|---|---|---|---|---|
| UiO-66-(A) | 1204 | 0.510 | 277 | 0.9995 |
| UiO-66-(B) | 1308 | 0.530 | 300 | 0.9995 |
| UiO-66-EDTA | 269 | 0.152 | 62 | 1.0000 |

Table 5-1. Calculated properties from BET curve equation of UiO-66 and modified UiO-66-EDTA

The BET surface areas of UiO-66-(A) and UiO-66-(B) are 1204 $m^2/g$ and 1308 $m^2/g$ respectively. The calculation for the BET surface area is shown in Appendix II. By comparing the BET surface area for the UiO-66 with the literature value, 1160 $m^2/g$, it can be concluded that the BET surface area of UiO-66-(A) and UiO-66-(B) are both slightly higher than the literature value of UiO-66. The two low-angle diffraction in PXRD indicated the missing cluster defects and the TGA showed missing linker defects therefore the synthesized material is defective. A surface area value higher than 1160 $m^2/g$ for a defective UiO-66 is expected and similarly observed in the literature by Shearer et al.(Shearer et al., 2016).

For UiO-66-EDTA the BET surface area is 269 $m^2/g$. This value is slightly lower than the literature value, 383.5 $m^2/g$, obtained by J. Wu et al. on UiO-66-EDTA. The BET surface area discloses that there are EDTA incorporated to the MOF. It is important to understand that the BET surface area of UiO-66-EDTA can vary depending on various factors, such as synthesis conditions and modifications.

UiO-66-((A) and (B)) and UiO-66-EDTA, have a significant difference by comparing their BET surface areas. The size of the molecules in both MOFs has a substantial impact, since larger molecules tend to often occupy more surface space than smaller molecules, which results in a reduction in the MOFs overall surface area. This is due to the fact that larger molecules occupy a higher amount of the available surface area owing to their lower surface-to volume ratio than smaller molecules.

The BET surface area of UiO-66-EDTA can also be impacted by the structure and shape of the MOF. UiO-66-EDTA has a complex structure which can make it unable to access all the available surface area.

### *5.2.5 Loading of functional groups*

Figure 5-6. below, is an $^{1}$H-NMR spectrum for UiO-66 and terephthalic acid, which indicates that there is linker presented in the MOF. The spectrum displays a weak doublet peak at around 2.1-2.2 and a singlet peak 8.4, which implies the presence of formate and dimethylamine which are contaminated products from the hydrolysis of base (NaOH) catalyzed DMF. $^{1}$H-NMR data for dimethylamine presents a doublet peak at 2.2 and 2.1 and for formate (the conjugate base of formic acid) usually displays a singlet peak at 8.4 (Shearer et al., 2016). The presence of terephthalic acid, can make the $^{1}$H-NMR spectrum of UiO-66 often displays broad signals. The resolution and sensitivity of the $^{1}$H-NMR spectrum could be constrained by this widening, which can result to changes in values (ppm) and size of peaks (Rehman et al., 2022).

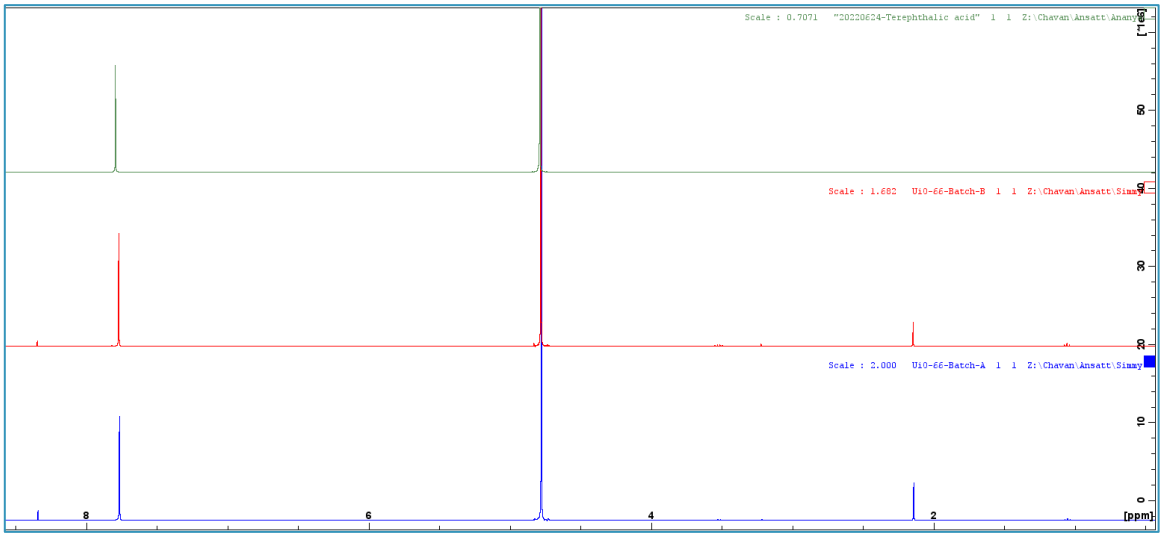


Figure 5-6. $^{1}$H-NMR data for UiO-66-(A) (blue spectrum), UiO-66-(B) (red spectrum) and terephthalic acid (green spectrum)

For UiO-66-EDTA the $^{1}$H-NMR spectrum below in Figure 5-7. confirms the modification with EDTA, and similar to UiO-66, shows the products from hydrolysis of DMF. Terephthalic acid is also present in the spectrum, which implies that the linkers are intact with the clusters. Due to the presence of terephthalic acid and EDTA the spectrum displays broad signals.

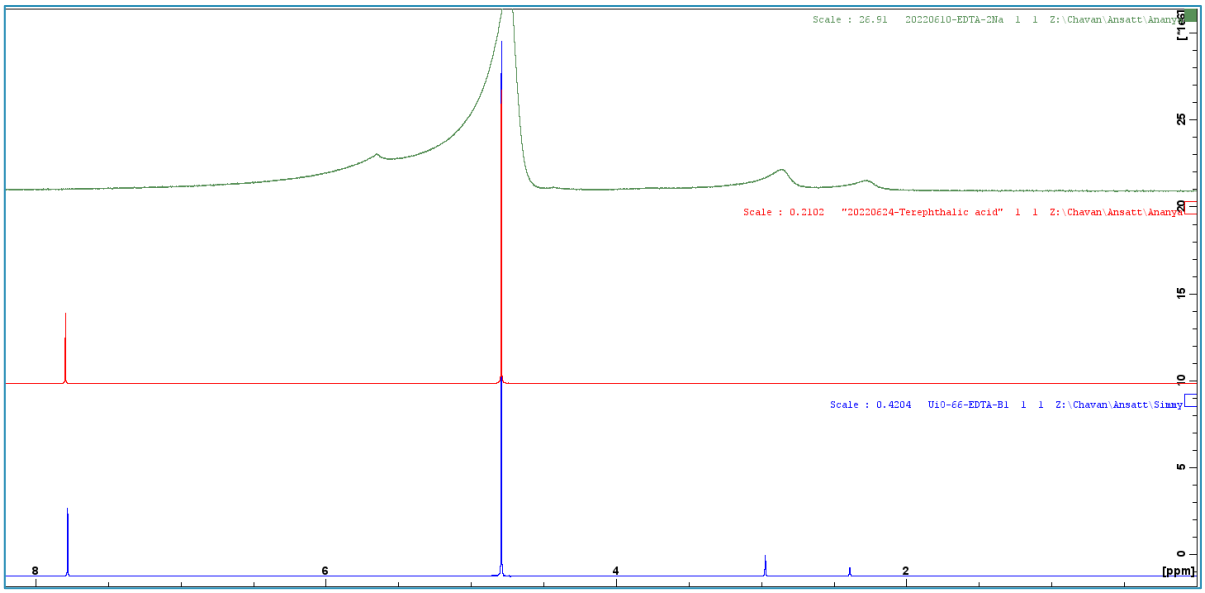


Figure 5-7. NMR spectrum for EDTA (green spectrum), terephthalic acid (red spectrum) and UiO-66-EDTA (blue spectrum)

The Table 5-2. provided below, is a summary of calculated molar ratio from Appendix III, that shows the total molar ratio of functional group (EDTA) compared to linker (BDC). The calculated molar ratio ($m_R$) is 0.25 with respect to $^1$HNMR data, but for more accurate quantification of EDTA one must an improved H-NMR method or an alternative technique.

| Sample | Linker | Functional groups (FG) | $(\frac{FG}{BDC})m_R$ | Total $m_R$ |
|---|---|---|---|---|
| UiO-66-EDTA | Terephthalic acid (BDC) | EDTA-2Na | 0.25 | 0.25 |

Table 5-2. NMR quantified molar ratio for UiO-66-EDTA

## 5.3 ADSORPTION EXPERIMENTS

### *5.3.1 Calibration curve for LiCl*

The IC (Ion Chromatography) was used to analyze lithium from simulated LiCl solutions. The calibration curve for LiCl is shown below in Figure 5-8. A linear trendline was drawn to fit the data set, which gave a correlation coefficient ($R^2$) of 0.996855. The negligeable inaccuracy comes from 2000 ppm LiCl.

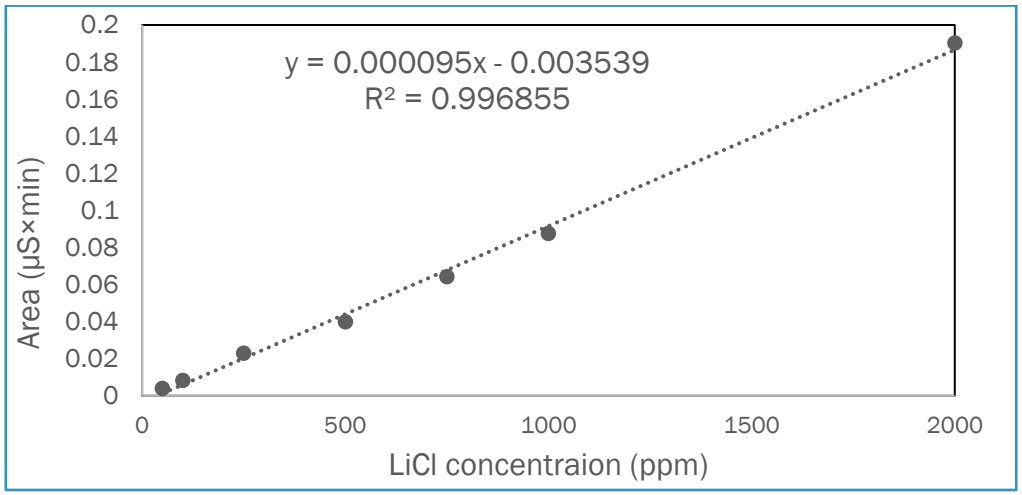


Figure 5-8 Calibration curve of simulated LiCl solution

### *5.3.2 Adsorption of $Li^+$*

The adsorption of lithium on both UiO-66 and UiO-66-EDTA was investigated from pH 5 until pH 12 at a fixed concentration of LiCl. The data after running adsorption showed no lithium uptake. An XRD-analysis was conducted to observe pattern and confirm the crystal structure of UiO-66 and UiO-66-EDTA after the adsorption. The XRD-patterns below in Figure 5-9 indicates that the crystal structures were not affected by the adsorption.

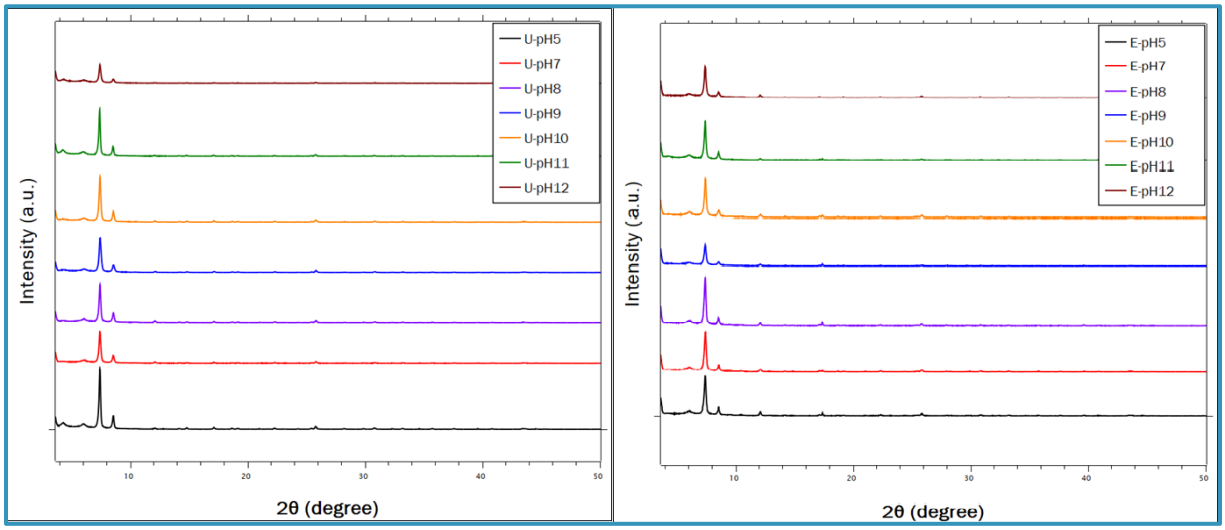


Figure 5-9. XRD pattern comparison of pH for UiO-66 (**left**) and UiO-66-EDTA (**right**) after adsorption

### 5.3.3 Adsorption of $Mg^{2+}$

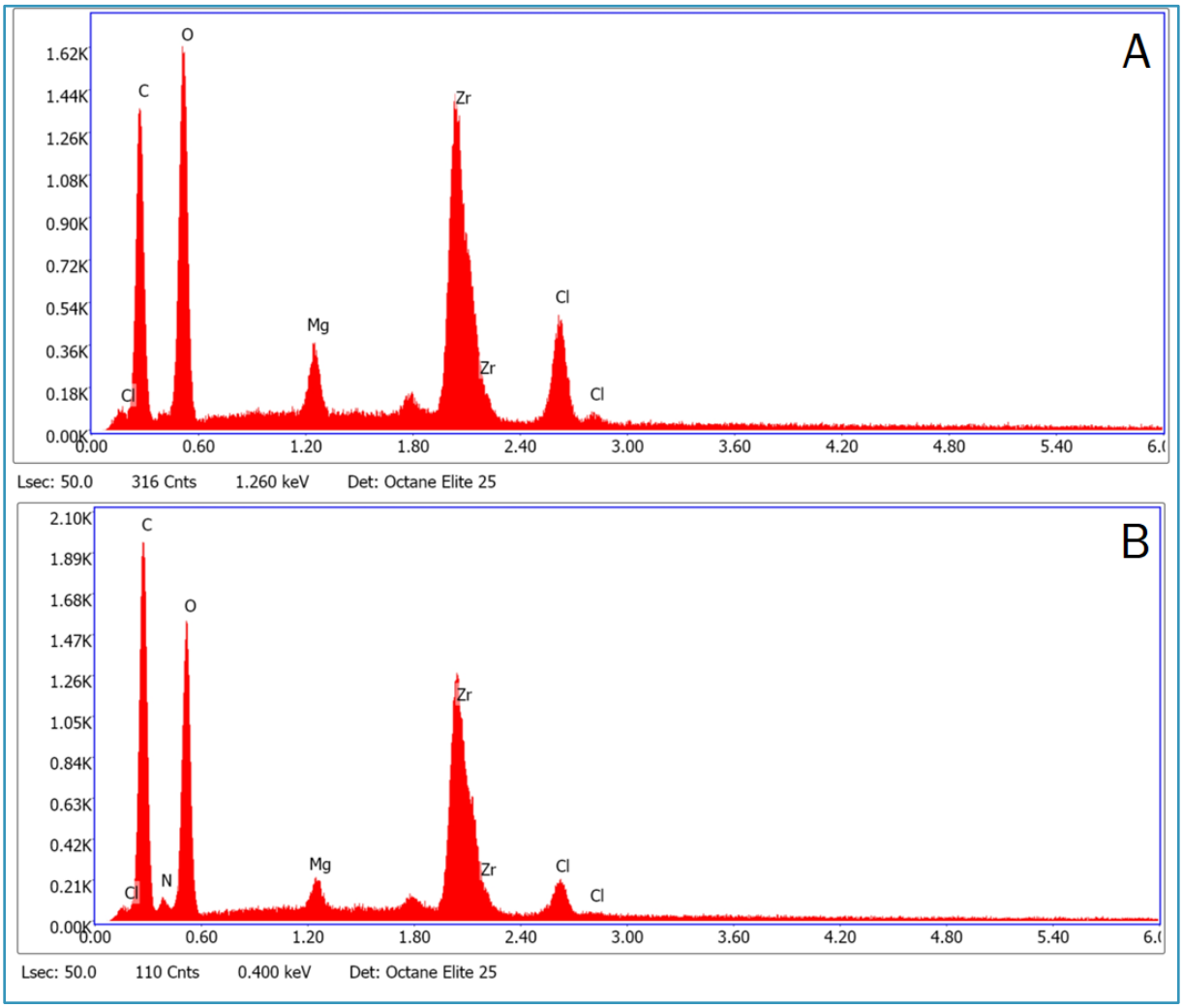


Figure 5-10. SEM analysis after adsorption of $Mg^{2+}$for UiO-66 (A) and UiO-66-EDTA (B)

The displayed EDS-analyzed graph above in Figure 5-10 and the summarized data below in Table 5-3. suggest the uptake of $Mg^{2+}$ in UiO-66 (A) and UiO-66-EDTA (B) after adsorption. By observing the EDS-data (A and B) and comparing the atomic percentage of zirconium and magnesium for UiO-66 and UiO-66-EDTA, the $Mg^{2+}$ uptake from the adsorption is higher for UiO-66 than for UiO-66-EDTA.

| Sample name | Weight % | | | Atomic % | | |
|---|---|---|---|---|---|---|
| | Zr | Cl | Mg | Zr | Cl | Mg |
| UiO-66 | 23.90 | 5.68 | 2.36 | 4.68 | 2.86 | 1.73 |
| UiO-66-EDTA | 21.59 | 2.39 | 1.30 | 3.94 | 1.12 | 0.89 |

Table 5-3. Summarized values of weight % and atom % from EDS analysis after adsorption with UiO-66 and UiO-66-EDTA

### *5.3.4 Adsorption of $Co^{2+}$ and $Ni^{2+}$*

The preparation of UV-visible spectrometer calibration curves of both cobalt and nickel was performed by a former master's student (Fernando, 2022), and the curves from the experiment are shown in Appendix V in Figure V-1. A linear trendline was drawn to fit the data set for both cobalt and nickel, which gave a correlation coefficient ($R^2$) of 0.99999 and 0.99996, respectively. Figures V-1 and V-2 in Appendix V show the SEM analysis spectra after the adsorption of both cobalt and nickel and in addition summarized values of weight % and atom % of the adsorbed MOFs from the EDS analysis are shown in Table V-1.

### *5.3.5 UV-analysis*

Cobalt (600 ppm) and nickel (2000 ppm) were observed at 510 nm and 394 nm respectively, to find the initial concentrations before adsorption by comparing the calibration curves of concentration and the absorbance, Tabled in Appendix V. With the initial concentrations and the measured data of absorbance from UV adsorption analysis of UiO-66 and UiO-66-EDTA for $Co^{2+}$ and $Ni^{2+}$, the equivalent concentration of absorbance and removal efficiency was calculated. which are presented below in Table 5-4.

| UV-samples | Absorbance | Equivalent conc. of abs. (mg/L) | Wavelength (nm) | Removal efficiency (%) |
|---|---|---|---|---|
| UiO-66-Co | 0.0475 | 579.23 | 394 | 0 |
| EDTA-Co | 0.0363 | 442.24 | 394 | 22.67 |
| UiO-66-Ni | 0.1827 | 1932.66 | 510 | 1.4 |
| EDTA-Ni | 0.1736 | 1836.38 | 510 | 6.32 |

Table 5-4. Data from UV adsorption analysis of UiO-66 and UiO-66-EDTA for $Co^{2+}$ and $Ni^{2+}$

The calculations for adsorption capacity are shown in Appendix V, which are calculated by using the data from the Table 5-4 above. Figure 5-11. below show the adsorption capacity (mg/g) of cobalt and nickel for UiO-66 and the modified UiO-66-EDTA.

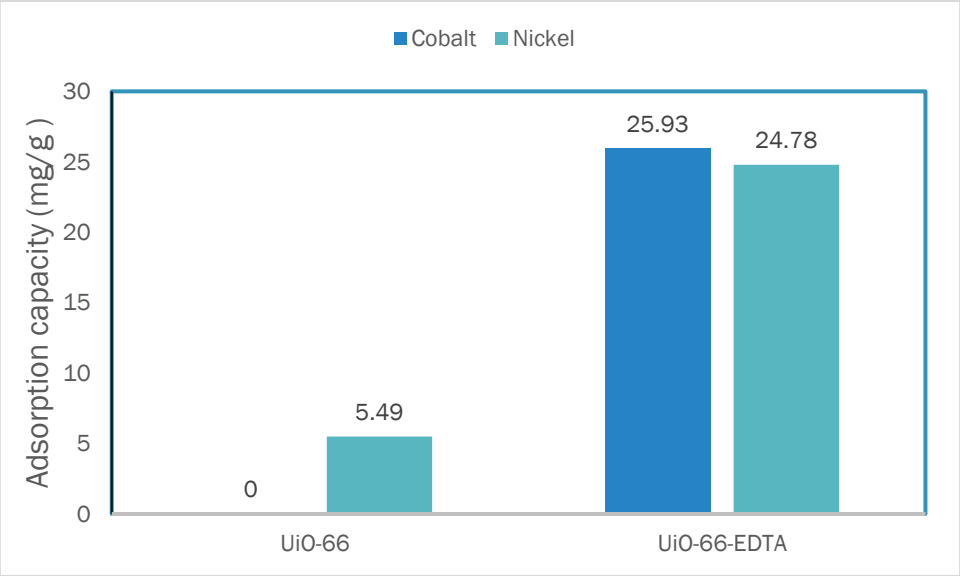


Figure 5-11. Adsorption capacity (mg/g) of UiO-66 and UiO-66-EDTA for cobalt (blue) and nickel (cyan)

UiO-66-EDTA showed a remarkably higher adsorption capacity than UiO-66 for $Co^{2+}$ and $Ni^{2+}$, as seen in the diagram. The EDTA group in UiO-66-EDTA provides more active sites where the divalent metal ions have bonded efficiently. UiO-66 had an adsorption capacity of 5.49 mg/g for $Ni^{2+}$, which traces back to the no presence of specific active functional groups to provide active sites for both the metal ions.

The metal uptake capacity we observed is much lower compared to what is reported in the literature by J. Wu et al. The difference in the metal uptake could be due to the lower loading of EDTA on UiO-66. However, J. Wu et al did not investigate both alkali and alkaline earth metal adsorption which is very important when adsorbents are developed for the recovery of critical metals from black mass leachate from the battery or separation from brine. The concentrations used in their review paper were neither optimized for the real concentration of black mass leachate from the battery nor for separation from brine. The exceptional selectivity for nickel, cobalt, and magnesium indicates that UiO-66 is a selectively binding divalent metal ion and shows no uptake of monovalent ions under similar conditions. (J. Wu et al., 2019)

That makes UiO-66-EDTA a very promising material for critical metal recovery from battery leachate and brine. Where $Li^{+}$ will be left in the solution while $Ni^{2+}$ and $Co^{2+}$ in the case of battery leachate and $Mg^{2+}$ in the case of brine will be adsorbed by UiO-66-EDTA. Of course, the metal uptake capacity which is directly linked to the loading of EDTA needs to be improved and optimized. If the capacities published in the literature are reproduced, then this will give a very promising adsorbent for separating monovalent and divalent cations.

# 6 CONCLUSION AND FUTURE WORK

The synthesis of a defective high surface area UiO-66 material and the modified UiO-66 (UiO-66-EDTA) with EDTA were successful. The characterization of UiO-66-EDTA; $^{1}$H-NMR and TGA revealed the loading on MOF, and XRD displayed the retained crystal structure of the MOF. This UiO-66-EDTA demonstrated low but selective uptake of divalent cations, such as $Mg^{2+}$, $Co^{2+}$ and $Ni^{2+}$, while revealed no uptake of monovalent cation like $Li^{+}$ which was observed under similar conditions. This makes UiO-66-EDTA a potential material to be further researched for separating Li (monovalent) from Ni, Co, and Mn (bivalent) in battery leachate. Also separating $Li^{+}$ from $Mg^{2+}$ in brine. We also notice some loss of EDTA during the adsorption therefore the process for loading EDTA on UiO-66-MOFs need further optimization to increase the loading inside the MOF.

Based on the present literature for UiO-66 and UiO-66-EDTA, it can be concluded that the MOFs are effective adsorbents for adsorption of divalent metals, and the experimented adsorption from this study demonstrated the reproducibility of the literature. In addition, in this study there was an attempt on adsorption of monovalent metal ions with UiO-66-EDTA which has not been published in literature, even though there have been reports with UiO-66. In entirety, the practical application of MOFs for adsorption processes continues to be researched and further study is required to completely understand the fundamental characteristics of adsorption in MOFs (UiO-66 and further modifications), and to improve the performance of these adsorbents for specific separations.

This study had its difficulties at the beginning due to unfamiliar literature and research methods, but after a significant amount of reading and understanding, the whole project seemed brighter. The newly developed technical skills during this time were handy for the unknown synthesis of MOFs, the operating of instruments for the characterization of those MOFs (XRD, TGA, SEM-EDS, N2-sorption), and especially the adsorption experiments. Based on unexpected challenges and setbacks which required different approaches and critical thinking gave a practical learning curve that can be applied in future research. Through these processes, the experience of significant growth in my intellectual and academic abilities, as well as a sense of accomplishment and confidence has given me the ability to pursue further studies or professional endeavors.

# REFERENCES


Alvial-Hein, G., Mahandra, H., & Ghahreman, A. (2021). Separation and recovery of cobalt and nickel from end of life products via solvent extraction technique: A review. *Journal of Cleaner Production*, *297*, 126592. https://doi.org/10.1016/j.jclepro.2021.126592

Aunan, E., Affolter, C. W., Olsbye, U., & Lillerud, K. P. (2021). Modulation of the Thermochemical Stability and Adsorptive Properties of MOF-808 by the Selection of Non-structural Ligands. *Chemistry of Materials*, *33*(4), 1471–1476. https://doi.org/10.1021/acs.chemmater.0c04823

Cavka, J. H., Jakobsen, S., Olsbye, U., Guillou, N., Lamberti, C., Bordiga, S., & Lillerud, K. P. (2008). A New Zirconium Inorganic Building Brick Forming Metal Organic Frameworks with Exceptional Stability. *Journal of the American Chemical Society*, *130*(42), 13850–13851. https://doi.org/10.1021/ja8057953

Costa, C. M., Barbosa, J. C., Gonçalves, R., Castro, H., Campo, F. J. D., & Lanceros-Méndez, S. (2021). Recycling and environmental issues of lithium-ion batteries: Advances, challenges and opportunities. *Energy Storage Materials*, *37*, 433–465. https://doi.org/10.1016/j.ensm.2021.02.032

*Critical raw materials*. (u.å.). Hentet 8. mai 2023, fra https://single-market-economy.ec.europa.eu/sectors/raw-materials/areas-specific-interest/critical-raw-materials_en

Falconnet, P. (1985). The economics of rare earths. *Journal of the Less Common Metals*, *111*(1), 9–15. https://doi.org/10.1016/0022-5088(85)90163-8

Fernando, J. S. R. (2022). *Selective Recovery of Nickel and Cobalt from Spent Battery Waste (Black Mass) by Adsorption: Resin and MOF Case Study* [Master thesis, uis]. https://uis.brage.unit.no/uis-xmlui/handle/11250/3022619

Furukawa, H., Cordova, K. E., O'Keeffe, M., & Yaghi, O. M. (2013). The chemistry and applications of metal-organic frameworks. *Science*, *341*(6149). Scopus. https://doi.org/10.1126/science.1230444

Ghosh, P., Colón, Y. J., & Snurr, R. Q. (2014). Water adsorption in UiO-66: The importance of defects. *Chemical Communications*, *50*(77), 11329–11331. https://doi.org/10.1039/C4CC04945D

Li, J.-R., Sculley, J., & Zhou, H.-C. (2012). Metal-organic frameworks for separations. *Chemical Reviews*, *112*(2), 869–932. Scopus. https://doi.org/10.1021/cr200190s

Meshram, P., Pandey, B. D., & Mankhand, T. R. (2014). Extraction of lithium from primary and secondary sources by pre-treatment, leaching and separation: A comprehensive review. *Hydrometallurgy*, *150*, 192–208. https://doi.org/10.1016/j.hydromet.2014.10.012

Rehman, S. ur, Xu, S., Xu, H., Tao, T., Li, Y., Yu, Z., Ma, K., Xu, W., & Wang, J. (2022). The Role of NMR in Metal Organic Frameworks: Deep Insights into Dynamics, Structure and Mapping of Functional Groups. *Materials Today Advances*, *16*, 100287. https://doi.org/10.1016/j.mtadv.2022.100287

Shearer, G. C., Chavan, S., Bordiga, S., Svelle, S., Olsbye, U., & Lillerud, K. P. (2016). Defect Engineering: Tuning the Porosity and Composition of the Metal–Organic Framework UiO-66 via Modulated Synthesis. *Chemistry of Materials*, *28*(11), 3749–3761. https://doi.org/10.1021/acs.chemmater.6b00602

Swain, B. (2017). Recovery and recycling of lithium: A review. *Separation and Purification Technology*, *172*, 388–403. https://doi.org/10.1016/j.seppur.2016.08.031

Tapia-Ruiz, N., Segalés, M., & Gregory, D. H. (2013). The chemistry of ternary and higher lithium nitrides. *Coordination Chemistry Reviews*, *257*(13), 1978–2014. https://doi.org/10.1016/j.ccr.2012.11.008

Wu, H., Chua, Y. S., Krungleviciute, V., Tyagi, M., Chen, P., Yildirim, T., & Zhou, W. (2013). Unusual and Highly Tunable Missing-Linker Defects in Zirconium Metal–Organic Framework UiO-66 and Their Important Effects on Gas Adsorption. *Journal of the American Chemical Society*, *135*(28), 10525–10532. https://doi.org/10.1021/ja404514r

Wu, J., Zhou, J., Zhang, S., Alsaedi, A., Hayat, T., Li, J., & Song, Y. (2019). Efficient removal of metal contaminants by EDTA modified MOF from aqueous solutions. *Journal of Colloid*

*and Interface Science*, *555*, 403–412. Scopus.

https://doi.org/10.1016/j.jcis.2019.07.108

# APPENDIX

## I. TGA

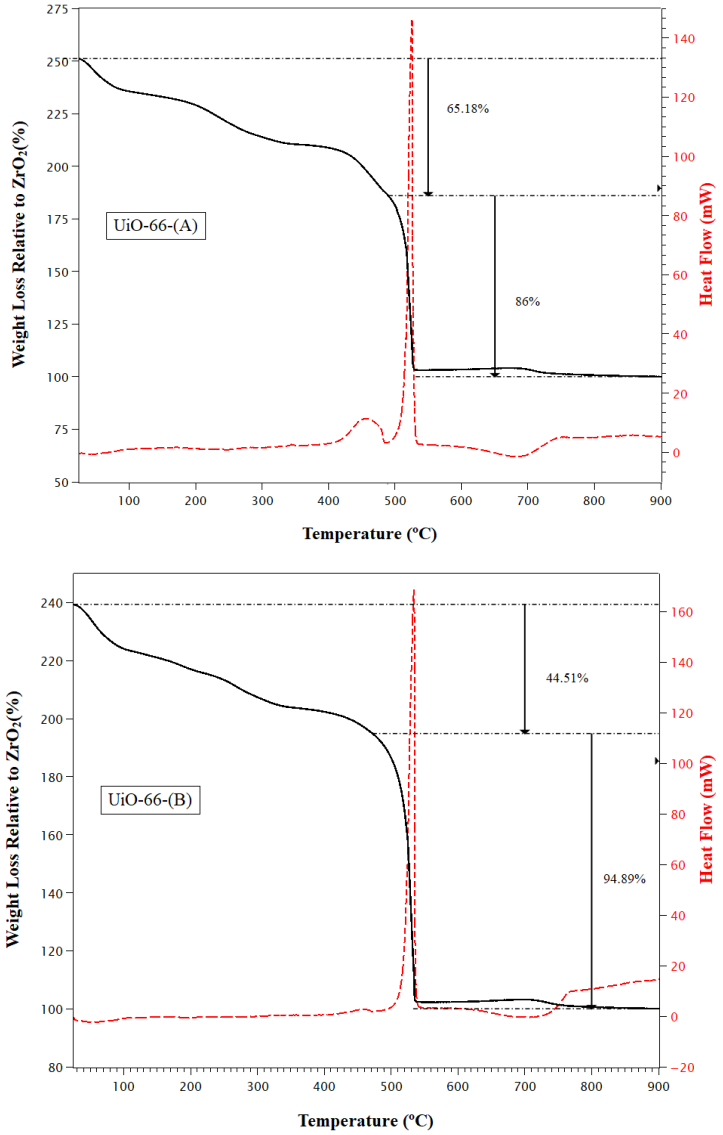


Figure I-1. Variation of weight loss % (black) and heat flow with time mW (red) for UiO-66-(A) (**on top**) and UiO-66-(B) (**on bottom**) with experimental weight plateau and weight end.

The calculations are based on Weight Plateau Theory and the determination of the molar ratios of functional groups presented in the modified UiO-66-EDTA. First, the Weight Plateau Theory, is used to calculate the weight contribution per BDC linker in UiO-66-EDTA.

The weight contribution per BDC linker (Weight Plateau Theory)

$$\text{Weight Plateau Theory} = \frac{\text{weight plateau ideal - weight end}}{N_A \text{ linker ideal}} = \frac{220.2\% - 100\%}{6} = 20.03\%$$

The Weight Plateau Ideal (220.2%) and Weight end (100%) values are determined experimentally from the $N_2$ sorption isotherm values. $N_A$ linker ideal, which is the number of BDC linkers in the theoretical UiO-66 structure, is assumed to be 6.

Weight Plateau Ideal = 220.2%
Weight end = 100%
$N_A$ linker ideal = 6

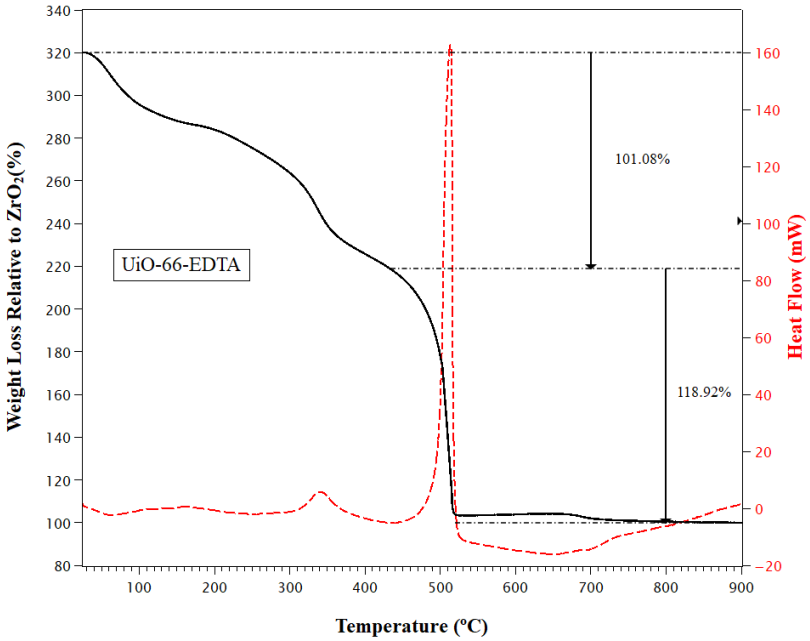


Figure I-2. Variation of weight loss % (black) and heat flow with time mW (red) for UiO-66-EDTA with experimental weight plateau and weight end.

HF: 3.12 mW
Ts: 486 C
Mass%: 186%

$N_A$ linker experimental = 6 – X

Based on the Weight Plateau Theory calculations, the $N_A$ linker experimental value is determined to be 5.9471.

$$N_A \text{ linker experimental} = 6 - X = \frac{\text{weight plateau experimental - weight end}}{\text{weight plateau ideal}} = \frac{118.92\%}{20.03\%} = 5.9371$$

$$6 - X = 5.9371$$
$$X = 0.0629$$

By inserting this value of X in $Zr_6O_{4+2X}(BDC)_{6-X}$, the molar mass of the UiO-66-EDTA sample is calculated as 1621.23 g/mol.

$$Mm\ (Zr_6O_{6.1258}(BDC)_{5.8742}) = 1621.23\ g/mol$$

$$\text{Weight Plateau Theory} = \frac{Mm\ (Zr_6O_{7.71}(BDC)_{4.29})}{Mm\ (6\ ZrO_2)} = \frac{1621.23\ g/mol}{739.34\ g/mol} \times 100\% = 219.28\%$$

The molar ratios of functional groups in the UiO-66-EDTA sample are determined by using the NMR spectroscopy data, which is provided in Appendix III. This ratio is then used, along with the value of $N_A$ linker experimental, to calculate the number of Y groups present in the sample of UiO-66-EDTA.

$$(\frac{FG}{BDC})m_R = \frac{2Y}{6 - X}$$

$$(\frac{FG}{BDC})m_R = \frac{\text{Integrated } H^1 \text{ of EDTA}}{N_A \text{ of } H^1 \text{ in EDTA}} \times \frac{\text{Integrated } H^1 \text{ of BDC}}{N_A \text{ of } H^1 \text{ in BDC}} = \frac{\text{Integrated } H^1 \text{ of EDTA}}{12} \times \frac{4}{4}$$

$$2Y = (6 - 0.0629) \times 0.25$$

$$2Y = 1.484275$$

$$Y = 0.7421375$$

Insert the calculated values of X and Y in $Zr_6O_{4+2x-2y}(OH)_{4-2x+2y}(BDC)_{6-x}(EDTA)_{2y}$:

This gives an approximated quantity of linker and functional groups according to experimental weight plateau of UiO-66-(A):

$$Zr_6O_{6.3475}(OH)_{6.3475}(BDC)_{4.29}(EDTA)_{1.0725}$$

## II. $N_2$ SORPTION

Calculation for BET surface area: UiO-66-(A)

y = 3608.4x + 6.7173

$$C = 1 + \frac{\text{gradient}}{\text{intercept}} = 1 + \frac{3608.4}{6.7173} = 538$$

$$V_M = \frac{1}{\text{slope} + \text{gradient}} = 0.000277\ m^3(STP)\ g^{-1}$$

$$V_M = 277\ cm^3(STP)\ g^{-1}$$

BET:

The data points used for the BET plot are compiled between a relative pressure range between 0.05 and 0.34, as this is the region displaying the best linear relation between the axes.

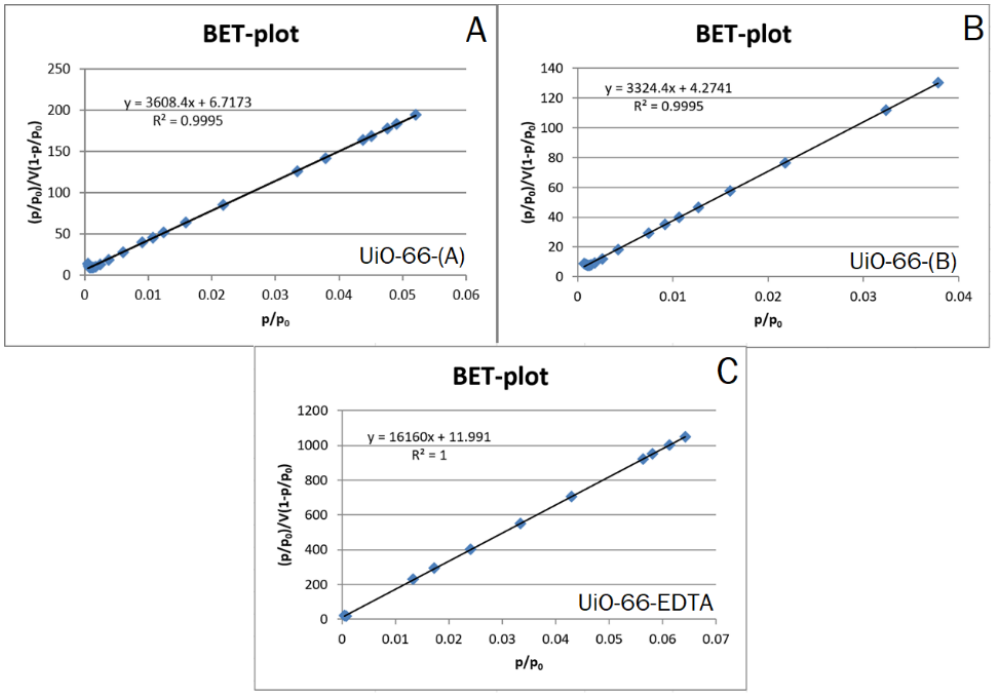


Figure II-1 BET plot for A (UiO-66-(A)), B (UiO-66-(B)) and C (UiO-66-EDTA)

BET surface area:

$$\text{BET surface area} = \frac{N_A P V_M}{RT} = 1204\ (m^3/g)$$

$N_A$: $6.022 \times 10^{23}$
P: 101325 Pa
$V_M$: 277 $cm^3(STP)\ g^{-1}$
R: $8.31451 \frac{J}{mol \times K}$
T: 273.15 K

# III. NMR

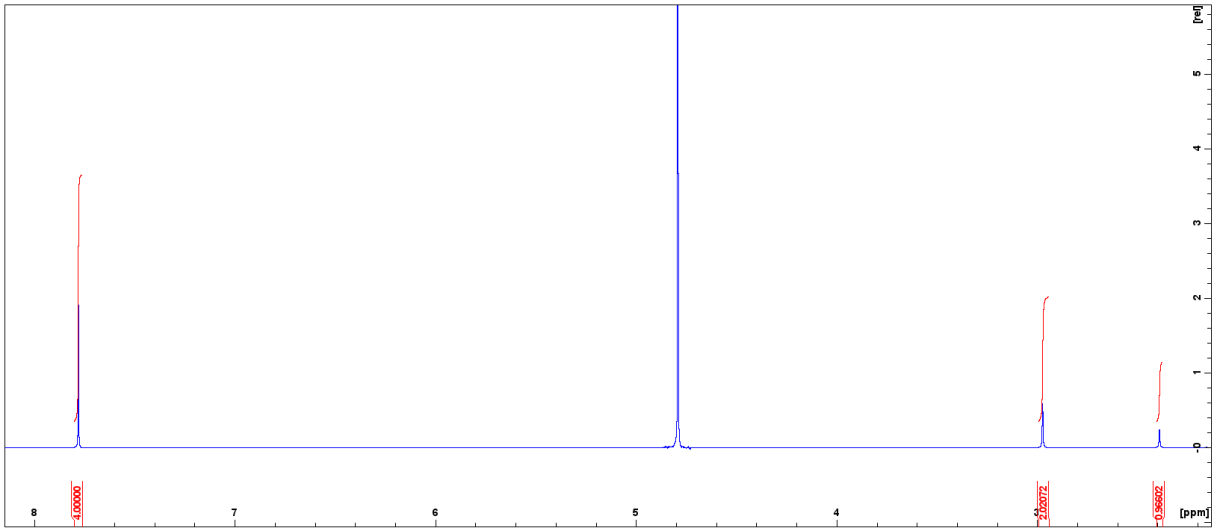


Figure III-1. NMR spectra with values for integrated $H^1$ of both EDTA and BDC

The ratio of the integrated $H^1$ signals of EDTA and BDC, which are provided above in Figure III-1, is used to calculate the ratio of the number of EDTA functional group in UiO-66-EDTA, by comparing with the $N_A$ of BDC in the MOF.

$$\left(\frac{FG}{BDC}\right)m_R = \frac{\frac{\text{Integrated } H^1 \text{ of EDTA}}{N_A \text{ of } H^1 \text{ in EDTA}}}{\frac{\text{Integrated } H^1 \text{ of BDC}}{N_A \text{ of } H^1 \text{ in BDC}}}$$

$$\left(\frac{FG}{BDC}\right)m_R = \frac{\text{Integrated } H^1 \text{ of EDTA}}{N_A \text{ of } H^1 \text{ in EDTA}} \times \frac{\text{Integrated } H^1 \text{ of BDC}}{N_A \text{ of } H^1 \text{ in BDC}}$$

$$\left(\frac{FG}{BDC}\right)m_R = \frac{\text{Integrated } H^1 \text{ of EDTA}}{12} \times \frac{4}{4} = 0.249435 \approx 0.25$$

# IV. ADSORPTION OF $Li^{2+}$

| Codes | pH before adsorption | pH after adding MOF |
|---|---|---|
| Blank-U | | 3.39 |
| U-5 | 5.06 | 3.72 |
| U-7 | 6.57 | 3.81 |
| U-8 | 8.03 | 3.89 |
| U-9 | 8.98 | 3.94 |
| U-10 | 9.99 | 3.98 |
| U-11 | 10.94 | 5.23 |
| U-12 | 11.98 | 10.91 |
| Blank-E | | 3.86 |
| E-5 | 4.99 | 3.73 |
| E-7 | 6.78 | 3.74 |
| E-8 | 8.01 | 3.79 |
| E-9 | 9.03 | 3.82 |
| E-10 | 9.98 | 3.88 |
| E-11 | 11.03 | 4.38 |
| E-12 | 12.04 | 5.58 |

Table IV-1 – Batch adsorption samples for $Li^{+}$ with pH measured before and after adding MOF (U = UiO-66-Batch-1 and E = UiO-66-EDTA)

## V. ADSORPTION OF $Ni^{2+}$ AND $Co^{2+}$

The calibration curve made from measurement done by UV-analyzing the simulated $Co^{2+}$ and $Ni^{2+}$.

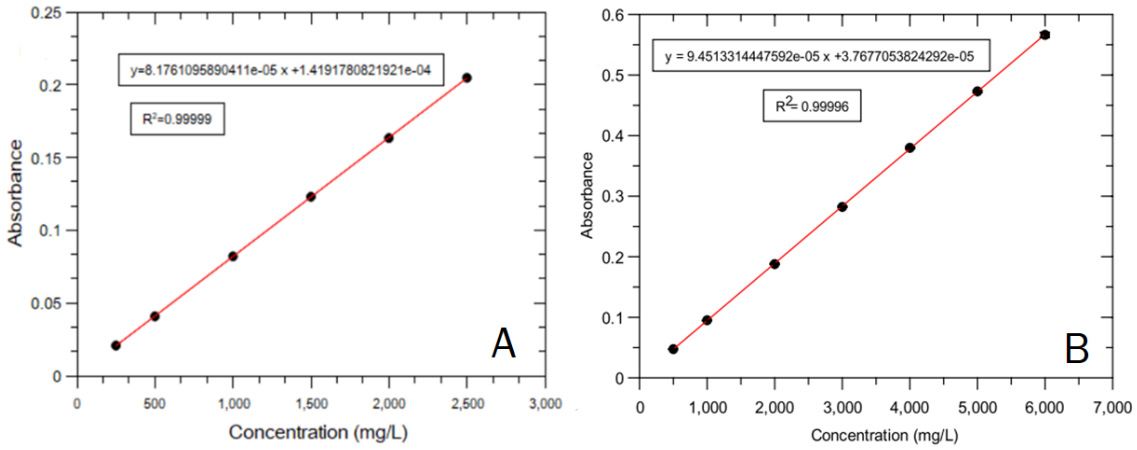


Figure V-1. Calibration curves of $Co^{2+}$ (A) and $Ni^{2+}$ (B)

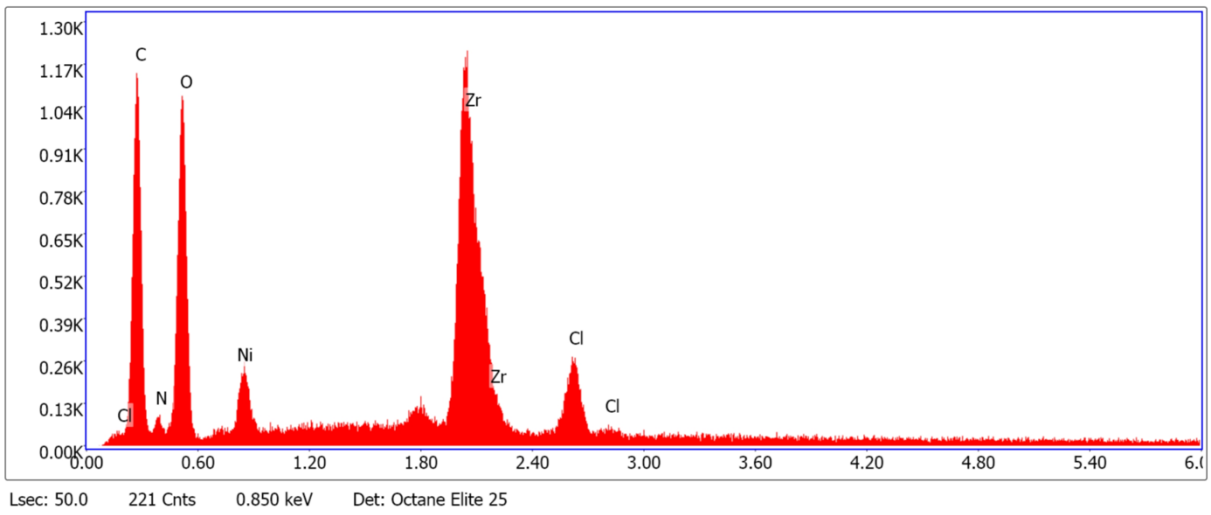


Figure V-2. EDS analysis of $Ni^{2+}$ adsorption with UiO-66-EDTA

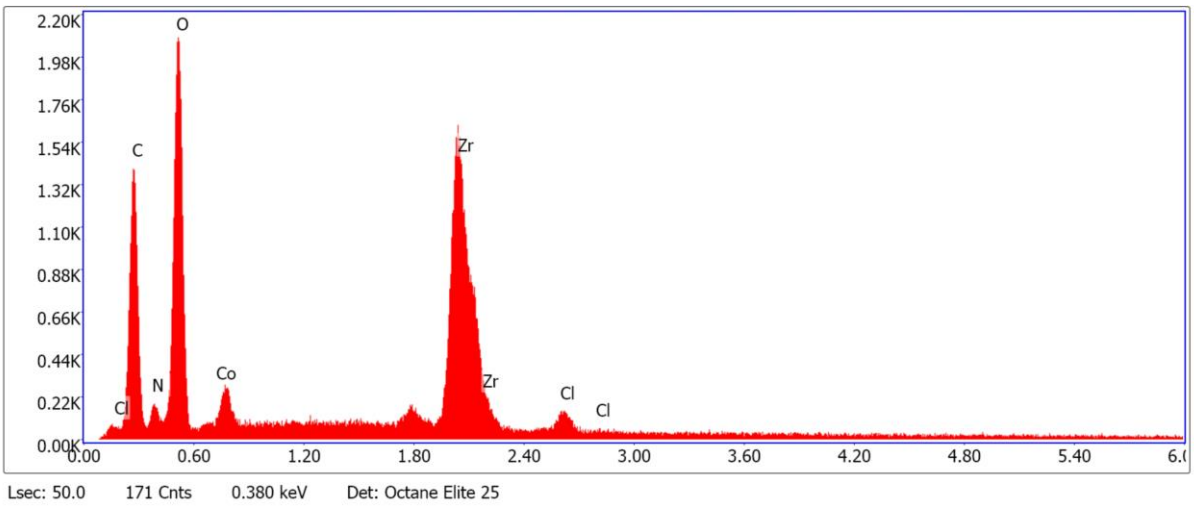


Figure V-2. EDS analysis of $Co^{2+}$ adsorption with UiO-66-EDTA

| Sample ID | Weight % | | | Atomic % | | |
|---|---|---|---|---|---|---|
| | Zr | N | Ni | Zr | N | Ni |
| E-Ni | 25.28 | 0.60 | 6.92 | 5.18 | 0.80 | 2.20 |
| | Zr | N | Co | Zr | N | Co |
| E-Co | 27.42 | 1.79 | 4.44 | 5.65 | 2.41 | 1.42 |

Table V-1. Summarized values of weight % and atom % from EDS analysis after adsorption with UiO-66-EDTA

Calculation for adsorption capacity (mg/g) of UiO-66 and UiO-66-EDTA for $Co^{2+}$ and $Ni^{2+}$, is presented below:

$$\text{Adsorption capacity} = \frac{\text{Initial sample conc.(mg/L)}}{\text{1000 mL}} \times \frac{\text{Removal efficiency \%}}{\text{100 \%}} \times \frac{\text{Volume soln. (mL)}}{\text{Amt of MOF (g)}}$$

| Initial sample | Absorbance | Wavelength |
|---|---|---|
| $Ni^{2+}$-2000 ppm | 0.1853 | 394 |
| $Co^{2+}$-600 ppm | 0.049 | 510 |

Table V-2. Adsorbance and wavelenghh of the initial samples

Calculating the removal efficiency, by inserting the initial concentration for either $Ni^{2+}$ at 2000 ppm or $Co^{2+}$ at 600 ppm shown above, and the calculated final concentration (the adsorbed sample):

$$\text{Removal efficiency \%} = \frac{\text{initial conc.- final conc.}}{\text{final conc.}} \times 100\ \%$$